Ordering of Hydrogen Bonds in High-Pressure Low-Temperature H_2O

Y. Q. Cai,[1,*] H.-K. Mao,[2] P. C. Chow,[1,†] J. S. Tse,[3] Y. Ma,[3] S. Patchkovskii,[3] J. F. Shu,[2] V. Struzhkin,[2] R. J. Hemley,[2] H. Ishii,[1] C. C. Chen,[1] I. Jarrige,[1] C. T. Chen,[1] S. R. Shieh,[4] E. P. Huang,[4] and C. C. Kao[5]

[1]*National Synchrotron Radiation Research Center, Hsinchu 30077, Taiwan*

[2]*Geophysical Laboratory, Carnegie Institution of Washington, Washington, D.C. 20015, USA*

[3]*Steacie Institute for Molecular Science, National Research Council of Canada, Ontario, K1A 0R6, Canada*

[4]*National Cheng Kung University, Tainan 701, Taiwan*

[5]*National Synchrotron Light Source, Brookhaven National Laboratory, Upton, New York 11937, USA*

(Received 11 August 2004; published 19 January 2005)

The near K-edge structure of oxygen in liquid water and ices III, II, and IX at 0.25 GPa and several low temperatures down to 4 K has been studied using inelastic x-ray scattering at 9884.7 eV with a total energy resolution of 305 and 175 meV. A marked decrease of the preedge intensity from the liquid phase and ice III to ices II and IX is attributed to ordering of the hydrogen bonds in the proton-ordered lattice of the latter phases. Density functional theory calculations including the influence of the Madelung potential of the ice IX crystal correctly account for the remaining preedge feature. Furthermore, we obtain spectroscopic evidence suggesting a possible new phase of ice at temperatures between 4 and 50 K.

DOI: 10.1103/PhysRevLett.94.025502 PACS numbers: 61.10.Ht, 64.70.Kb, 81.30.–t

The hydrogen bonds linking the water molecules are known to give rise to a rich variety of stable and metastable phases of H_2O under specific temperature and pressure conditions (Fig. 1) [1–7]. On the atomic level, the hydrogen bonds are formed between the H $1s$ electrons and a lone pair of electrons of the water molecules. The study of the electronic structure of the hydrogen bonds in various phases of H_2O therefore holds the key to understanding the change of hydrogen, covalent, and ionic bonding of the H_2O framework that is essential for understanding the icy planetary interiors as well as the physical and chemical properties of organic and biological systems at high pressure.

Analysis of the near-edge fine structure from x-ray absorption spectroscopy (XAS) provides much of the needed information [8], and was applied recently to liquid water at the oxygen K edge [9–11]. X-ray emission spectroscopy was also used to derive similar information [12]. Combined with first principles density functional calculations, the preedge region of the oxygen K edge absorption spectrum was identified to be associated with water molecules with uncoordinated donor hydrogen bonds, whereas the main edge and postedge regions were mainly related to fully coordinated molecules [9–11]. These studies thus provided crucial information on the bonding structure of the water molecules in liquid water on the subfemtosecond time scale of the x-ray absorption and emission processes.

Nevertheless, the submicron penetration depth of the soft x rays for probing the oxygen K edge ($\sim$540 eV) introduces uncertainties due to the surface sensitivity and is incompatible with the high-pressure environment necessary for the study of the high-pressure phases of H_2O. An alternative technique, based on the inelastic scattering of hard x rays ($\sim$ 10 keV) by core-level excitations, was used recently to study both the extended and the near-edge structures of the oxygen K edge in liquid water and ice under ambient conditions with a total energy resolution of $\sim$1 eV [11,13,14]. This technique, called x-ray Raman scattering (XRS), provides the same information as XAS when the momentum transfer of the XRS measurement is small enough that the dipole approximation is valid [15]. Its inherent bulk sensitivity and good penetration depth make it especially valuable for the investigation of samples under extreme thermodynamical conditions such as high pressure.

In this Letter, we report the first XRS measurement of the near K-edge structure of oxygen in liquid water and ices III, II, and IX at 0.25 GPa and several low temperatures (Fig. 1) down to 4 K with a much-improved total energy resolution of 305 and 175 meV at 9884.7 eV. The results reveal clearly the preedge feature and show spectral changes in the preedge, main edge, and postedge regions across the various phases, which can be understood based on the structure of the known ice phases and density func-

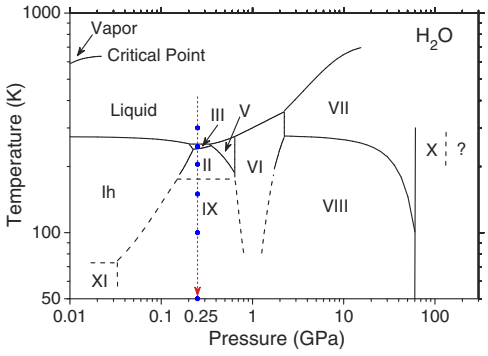

FIG. 1 (color online). Phase diagram of H_2O. The dashed arrow and the solid dots indicate the pressure and temperature path of the present measurements.

tional theory (DFT) calculations. Furthermore, we obtain evidence suggesting a possible new phase of ice at temperatures between 4 and 50 K.

The measurement was carried out on the Taiwan Beamline BL12XU at SPring-8 in Japan, dedicated to inelastic x-ray scattering (IXS) experiments on electronic excitations. The optical layout and the spectrometer are detailed in Ref. [16]. The total energy resolution of 305 and 175 meV (FWHM of the quasielastic lines off the sample) was achieved, respectively, using two 2-m radius Si(555) spherical analyzers, one with the Si wafer continuously bent and the other with strain-relief dicing [17], in combination with a Si(400) high-resolution monochromator at 9884.7 eV.

The sample was doubly distilled deionized water confined by a Be gasket and pressurized to 0.25 GPa using a Merrill-Bassett diamond anvil cell (DAC). The pressure was determined by measuring the ruby R_1 fluorescence wavelength [18] both before and after the XRS measurement. The sample volume was 1.6 mm diameter $\times 0.5$ mm height. Vibration-free cooling to 4 K was provided by a custom-built cryostat employing Cryomech's pulse-tube cryorefrigerator PT407. The temperature was measured by a calibrated Si diode placed near the DAC within a He-filled Be can. For comparison, measurement was also taken on liquid water under ambient conditions, in which a 2-mm thick cell filled with Wako Ultrapure water with 12.5 μm thick Kapton windows was used.

Figure 2 summarizes the data obtained with the energy resolution of (a) 305 and (b) 175 meV. The second data set was taken in a separate run to identify detailed changes in the near-edge region between 4 and 150 K in 50 K step. The cooling rate between two successive temperatures was ~ 3 K/min. Both the incident and scattered x rays went through the Be gasket. The scattering angle was fixed at 35°, corresponding to a momentum transfer $Q \sim 30$ nm^{-1} which satisfies the dipole condition $Qr_1 \sim 0.2 < 1$ ($r_1 = a_0/Z \sim 0.007$ nm is the radial extent of the oxygen $1s$ wave function). The momentum resolution was 2.3 nm^{-1}. All spectra shown are raw data normalized to the incident beam intensity. Total accumulated counts for the main peak were $\sim$600 (300) with 305 (175) meV resolution at a count rate of ~ 1 (0.5) count/s, of which about one-third was from background contributions dominated by the tail of the Compton profile of the valence electrons [15]. For comparison between the phases, the intensities have been scaled to the same integrated area between 535 and 545 eV above a horizontal baseline (indicated by a 0 for each spectrum).

Similar to previous XAS and XRS studies [9–11,13,14], the observed features can be divided into three regions: the preedge (535–537 eV), the main edge (537–540 eV), and the postedge (540–545 eV). We consider first the case of liquid water. Under atmospheric pressure and 0.25 GPa at 300 K, liquid water displays similar near-edge structures with a prominent preedge feature just above 535 eV, followed by an intense main edge peak at 538 eV and a broader postedge shoulder at 541 eV. Discernible pressure-dependent effects include a slight increase of the preedge intensity and the shifting of the main edge towards higher energy at 0.25 GPa. These changes are consistent with density functional calculations for liquid water and ice [9–11], the results of which showed that fully coordinated water molecules contribute only to the main edge and postedge regions through excitations to unoccupied oxygen $2p$ orbitals at 537.5 eV and to the conduction band centered at 541 eV. Molecules with an uncoordinated (broken or distorted) acceptor hydrogen bond at the oxygen site produce a similar near-edge spectrum, with additional intensity only between the main edge and postedge re-

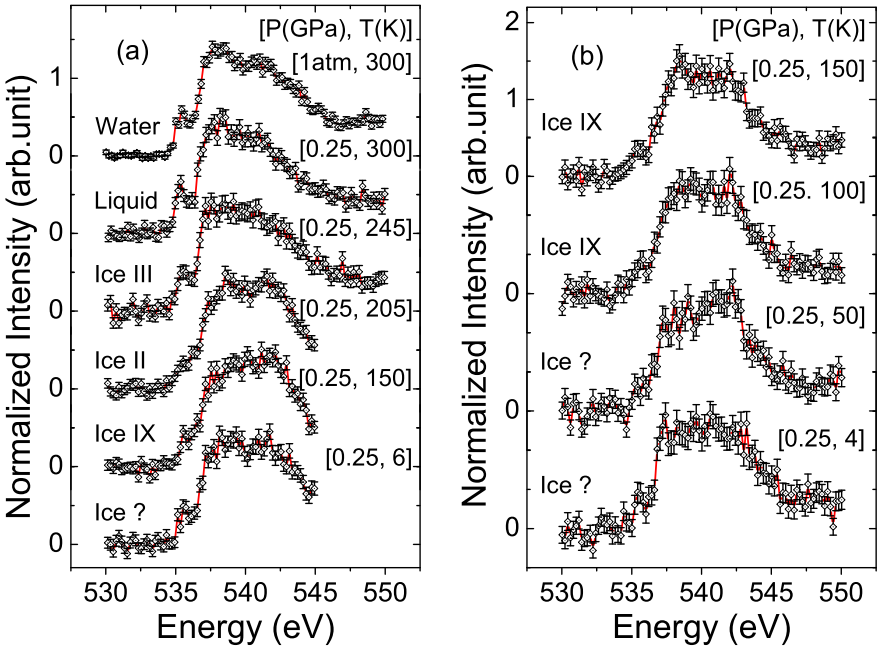

FIG. 2 (color online). Near K-edge spectra of the oxygen obtained with a total energy resolution of (a) 305 and (b) 175 meV. The phases and the pressure and temperature conditions are indicated.

gions. In contrast, molecules with an uncoordinated donor hydrogen bond at one of the hydrogen sites show a large orbital asymmetry, which leads to oxygen $2p$ and $2s$ orbital mixing that produces a strong discrete preedge peak, and a strong feature at the bottom of the conduction band that modifies the shape of the main edge and postedge regions of the spectrum. Therefore, the observed pressure-dependent changes of the near-edge structure in liquid water are most likely caused by an increase in uncoordinated hydrogen bonds in liquid water induced by high-pressure compression.

Changes in the near K-edge structure of oxygen in the ice phases can be understood qualitatively in a similar way. From the liquid phase to ice III at 0.25 GPa, for instance, the decrease of the preedge and main edge intensities seen in Fig. 2(a) is a consequence of the ordering of the oxygen framework and the partial ordering ($\sim$25%) of the protons in the lattice of ice III [19], which reduce the number of uncoordinated hydrogen bonds. From ice III to ices II and IX, this trend continues more dramatically, showing a marked decrease of the preedge intensity, accompanied by reduction (or growth) of the main edge (or postedge) intensity. The energy of the main edge and postedge features also shifts to higher energy by $\sim$0.8 eV. Ice IX is the low-temperature proton-ordered phase of ice III with an identical tetragonal crystal structure [19], whereas ice II has a *completely* proton-ordered rhombohedral lattice [20]. Within the local environment of the water molecules, the main structural difference between ice III and ices II and IX is therefore the degree of ordering of the protons or, more precisely, the ordering of the hydrogen bonds. The observed marked decrease of the preedge intensity is therefore a result of the diminishing number of uncoordinated hydrogen bonds in the proton-ordered lattice of ices II and IX.

We note that the ordering of protons in ice IX is not complete with $\sim$8% disordering [19]. Ice II is therefore more ordered than ice IX, which explains the slight increase of the preedge intensity from ice II to ice IX. The main edge and postedge features are also better resolved in ice II. We also note that the two data sets for ice IX at 150 K in Fig. 2 show different ratios of the main edge to the postedge intensities. This may be partly due to the poorer statistics of the second data set [Fig. 2(b)]. Another possibility, which is more likely, may be due to sample history. In measuring the second data set, the sample was cooled directly from 300 to 150 K without stopping at temperatures for measurements on ices III and II. This resulted in ice III being transformed directly into ice IX without going though ice II [19]. The sample history was found to affect the lattice constant of ice IX, and hence the bond length and angles of the water molecules, which could be related to the degree of hydrogen bond ordering in the lattice. The main edge and postedge intensities have been shown to be sensitive to such variations [11].

The remaining preedge intensities in ices II and IX are, however, unexpected as all (most) of the water molecules in the proton-ordered lattice of ice II (IX) are fully coordinated with symmetric hydrogen bonds, which should lead to diminishing preedge intensity based on the aforementioned molecular dynamics simulations [9–11]. We have performed DFT calculations of the near-edge XAS spectrum of ice IX, and found that the remaining intensity may be due to the influence of the local electronic structure by the Madelung potential of the crystal lattice.

The calculation was based on ice IX cluster models generated using ordered crystal structure IX of Ref. [19]. For the two crystallographically distinct oxygen sites (O1 and O2) in ice IX, all water molecules within a cutoff radius of R_c were included explicitly in the electronic structure calculation. R_c was selected in the range of 7–8 Å so that the total TIP3P dipole moment of the cluster was minimized. The influence of the Madelung potential of the ice IX crystal was then estimated by surrounding each cluster with point charges placed at the hydrogen and oxygen periodic lattice positions, with the magnitude of the charges screened to reproduce the Madelung potential of the infinite periodic lattice of ice IX [21].

Incorporation of the Madelung potential leads to a significant increase in the band gap of the quantum mechanical cluster, from 2.8 (2.4) eV for the bare O1 (O2) cluster models, to 5.1 (4.9) eV for the same clusters in the Madelung potential. This change is accompanied by a significant reduction in the surface contribution to the states close to the Fermi level, making these states more localized. Calculations of the near-edge XAS spectrum were performed using the Slater transition potential approach [22] within the dipole approximation. The calculated continuum ionization threshold is 538.0 (538.3) eV for the O1 (O2) site. For transitions above 550.1 eV, calculated absorption lines were broadened using the Gaussian line shape of 4.5 eV FWHM. For transitions below 540.1 eV, a 0.5 eV linewidth was used. In the intermediate region, the linewidth was interpolated linearly between the two limiting values [22]. The overall XAS spectrum was then calculated as a 2:1 weighted average of the O1 and O2 site spectra, accounting for the 2:1 ratio between the number of the O1 and O2 sites in ice IX.

The calculated XAS spectrum including the point charges reproduces well all the major features of the experimental spectrum (see Fig. 3), although quantitative agreement between the calculated and observed spectrum is less satisfactory. The discrepancy may be due to the neglect of multielectron excitations near the ionization threshold and vibrational effects, which may result in additional but weak features not considered here. Compared to the spectrum calculated without the point charges, inclusion of the point charges introduces intensity in the preedge region (the shaded area in Fig. 3) which mimics the shape of the experimental curve rather well. We therefore conclude that the Madelung potential of the ice IX lattice causes the remaining preedge intensity in the near-edge spectrum. A similar situation may be expected for ice II. This is in contrast to liquid water where the near-edge

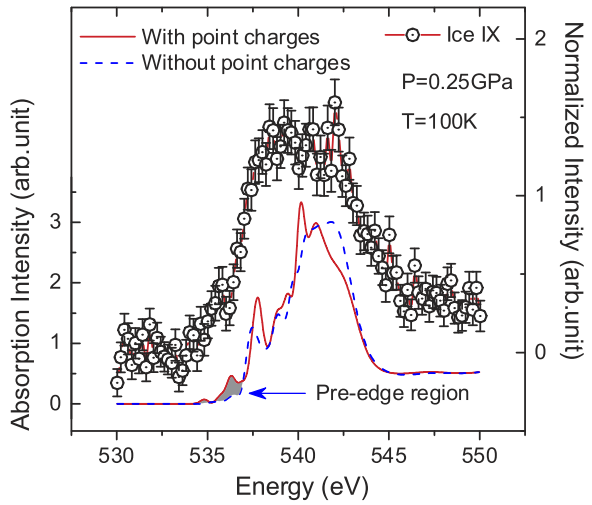

FIG. 3 (color online). Comparison of near K-edge spectra of ice IX with DFT calculations. The shaded area indicates the difference in the preedge region of the calculation with and without the point charges.

structure is determined predominantly by the first coordination shell of the water molecules [11]. These results can be reconciled, however, by considering that the ordered proton network creates a long-range anisotropy in the H_2O framework and introduces the necessary orbital asymmetry in the hydrogen bonds of the water molecules, causing the observed preedge intensity. A randomly distributed proton network smears out the anisotropy, and the preedge intensity is dominated by uncoordinated donor hydrogen bonds.

Finally, we examine the temperature-dependent behavior between 4 and 150 K presented in Fig. 2(b). Given the similarity between the spectra at 150 and 100 K, the ice IX phase existed at least down to 100 K. At 50 K, the main edge began to sharpen and eventually led to a pronounced preedge feature and a sharp main edge peak at ~537 eV at 4 K. There is a possibility that the sharpening of the main edge feature is due to reduced vibration amplitude at low temperature, accompanied by increased ordering of the protons in the ice IX lattice. The growth of the preedge intensity, however, contradicts this possibility based on the trend observed in Fig. 2(a). The results therefore suggest a possible new phase at temperatures between 4 and 50 K. The overall variations in the intensity and/or energy of the preedge, main edge, and postedge features compared to those of ice IX are substantial, which implies substantial changes in the H_2O framework. Further structural characterization is required to confirm the finding.

In conclusion, we have studied the near K-edge structure of oxygen in liquid water and ices III, II, and IX at 0.25 GPa and various low temperatures down to 4 K for the first time using inelastic x-ray scattering with high energy resolutions. The observed spectral details coupled with density functional theory calculations indicate that the Madelung potential of the proton-ordered lattice contributes also to the preedge intensity. At temperatures between 4 and 50 K, spectroscopic evidence is presented suggesting the existence of a possible new phase of ice. The present work further demonstrates the potential of the IXS technique for studying materials under extreme conditions of pressure and temperature.

Y. Q. C. is grateful to Dr. T. Ishikawa for support. This work was carried out at SPring-8 under experiments No. C03A12XU-1504N and No. C04A12XU-1500N, and was partly supported by NSRRC and the NSC of Taiwan under Grant No. NSC 92-2112-M-213-012. The Carnegie group is grateful to NSF-DMR, DOE (BES, NNSA-CDAC), and NASA for support.

*Electronic address: cai@nsrrc.org.tw
†Present address: HP-CAT, Advanced Photon Source, Argonne National Laboratory, Argonne, IL 60439, USA.

[1] P. V. Hobbs, *Ice Physics* (Clarendon, Oxford, 1974).
[2] W. B. Hubbard, *Planetary Interiors* (Van Nostrand Reinhold, New York, 1984).
[3] A. Polian and M. Grimsditch, Phys. Rev. Lett. **52**, 1312 (1984).
[4] O. Mishima, L. D. Calvert, and E. Whalley, Nature (London) **310**, 393 (1984); **314**, 76 (1985); O. Mishima, K. Takemura, and K. Aoki, Science **254**, 406 (1991).
[5] R. J. Hemley *et al.*, Nature (London) **330**, 737 (1987); R. J. Hemley, L. C. Chen, and H. K. Mao, Nature (London) **338**, 638 (1989).
[6] C. Lobban, J. L. Finney, and W. F. Kuhs, Nature (London) **391**, 268 (1998).
[7] I. M. Chou *et al.*, Science **281**, 809 (1998).
[8] J. Stöhr, *NEXAFS Spectroscopy* (Springer-Verlag, Berlin, 1992).
[9] S. Myneni *et al.*, J. Phys. Condens. Matter **14**, L213 (2002).
[10] M. Cavalleri *et al.*, Chem. Phys. Lett. **364**, 363 (2002).
[11] Ph. Wernet *et al.*, Science **304**, 995 (2004).
[12] J.-H. Guo *et al.*, Phys. Rev. Lett. **89**, 137402 (2002).
[13] D. T. Bowron *et al.*, Phys. Rev. B **62**, R9223 (2000).
[14] U. Bergmann *et al.*, Phys. Rev. B **66**, 092107 (2002).
[15] Y. Mizuno and Y. Ohmura, J. Phys. Soc. Jpn. **22**, 445 (1967). For recent reviews on the status of XRS and discussions of the theoretical framework, see M. Krisch and F. Sette, Surf. Rev. Lett. **9**, 969 (2002); U. Bergmann, P. Glatzel, and S. P. Cramer, Microchemical J. **71**, 221 (2002).
[16] Y. Q. Cai *et al.*, in *Synchrotron Radiation Instrumentation: Eighth International Conference on Synchrotron Radiation Instrumentation*, AIP Conf. Proc. No. 705 (AIP, New York, 2004), p. 340.
[17] D. J. Wang *et al.*, in *Synchrotron Radiation Instrumentation: Eighth International Conference on Synchrotron Radiation Instrumentation* (Ref. [16]), p. 869.
[18] H. K. Mao *et al.*, J. Appl. Phys. **49**, 3276 (1978).
[19] J. D. Londono, W. F. Kuhs, and J. L. Finney, J. Chem. Phys. **98**, 4878 (1993).
[20] G. J. Wilson *et al.*, J. Chem. Phys. **43**, 2384 (1965).
[21] G. te Velde and E. J. Baerends, Phys. Rev. B **44**, 7888 (1991).
[22] L. Triguero, L. G. M. Pettersson, and H. Ågren, Phys. Rev. B **58**, 8097 (1998).